MODEL IMAGES OF RADIO HALOS AROUND SUPERNOVA REMNANTS

STEPHEN P. REYNOLDS
Physics Department, North Carolina State University, Raleigh, NC 27695
Received 1993 February 26; accepted 1993 July 9

ABSTRACT

I present model calculations of profiles and two-dimensional images of the radio synchrotron emission of young supernova remnants, concentrating on observable effects of relativistic electrons diffusing upstream of the shock wave. If the preshock electron scattering mean free path is sufficiently long, observable synchrotron halos outside the bulk of the radio emission can potentially result; their absence can constrain the mean free path from above. If scattering is primarily due, as expected, to Alfvén waves with amplitude δB, the halo is expected to extend a distance of order $r_g c (\delta B / B)^{-2}/v_s$ beyond the shock, where r_g is the gyroradius of the electrons emitting at the observed frequency, B is the upstream magnetic field strength, v_s is the shock velocity, and the amplitude δB refers to waves with wavelength comparable to r_g, of order 10^{13} cm for typical supernova-remnant parameters. However, the detailed geometry of the halo varies with the assumptions about particle acceleration in the shock wave. I present an atlas of model profiles and images as a function of preshock diffusion length, of aspect angle between the magnetic field and the line of sight, and of other relevant parameters.

Subject headings: radiation mechanisms: miscellaneous — shock waves — supernova remnants

I. INTRODUCTION

In standard Fermi shock acceleration theory, particles are scattered back and forth repeatedly across a shock front, presumably by magnetic fluctuations such as Alfvén waves, and gain energy before being convected away downstream. (See Blandford & Eichler 1987 or Jones & Ellison 1991 for recent reviews of shock acceleration.) Given a mean free path λ and a shock velocity v_s, particles will diffuse a distance of order $\lambda c / 3v_s$, the "diffusion length," upstream of the shock before being turned around by repeated scatterings to recross the shock. If relativistic, synchrotron-emitting electrons are accelerated in this way in shock waves in supernova remnants (SNRs), they will radiate upstream as well as downstream and cause the profile of SNR radio emission to ramp up smoothly rather than appear suddenly at the shock wave. The scale length of this ramp or precursor will be roughly the diffusion length of the electrons emitting at the frequency being observed, and will vary inversely with the intensity of Alfvén waves with wavelengths comparable to the gyroradii of those electrons. Since the shock wave probably compresses magnetic field as well as accelerating particles, a sharp turn-on of radio emission would result in the absence of this precursor; thus supernova remnants observed to have well-defined edges constrain the presence of such halos, and hence the scattering properties of the upstream medium.

The appearance of these predicted synchrotron halos depends on the properties of the upstream magnetic field, several assumptions about particle acceleration in the shock wave, and, to a lesser extent, on the postshock dynamics of the SNR. However, I shall show that unless the magnetic field external to the SNR is nearly along the line of sight, halos unlike any SNR morphology ever observed result unless the diffusion length for electrons with gyroradii of order 10^{13} cm is less than a few percent of the SNR radius. Quantitative application of these results to several well-observed SNRs is made in Achterberg,

Blandford, & Reynolds (1993, hereafter ABR) in which it is shown that the intensity of the resonant wave field near those SNRs must be higher by about three orders of magnitude or more than in the interstellar medium at large, whose properties are inferred by observations of Galactic cosmic rays. Such a result is expected in nonlinear theories of Fermi shock acceleration (e.g., Bell 1978; Blandford & Ostriker 1978) in which the upstream waves that scatter particles and return them to the shock are generated by those particles themselves. Further careful, high-resolution observations at several frequencies of young SNRs can fix or provide lower limits to the amplitude of waves at several length scales.

In § 2 I shall describe the general assumptions of these calculations, and the details of the calculations of model profiles and two-dimensional images. I present the results in § 3: profiles and images for a range of parameters and model types. Section 4 discusses some of the properties of these models, and how they may be compared with observations; § 5 brings a summary and conclusions. Earlier applications of model images of SNR synchrotron emission were made in Fulbright & Reynolds (1990, hereafter FR90) and Reynolds & Fulbright (1990, hereafter RF90); the technique has wide applications to the understanding of the nature of particle acceleration and other processes in supernova remnants.

2. CALCULATION

My model supernova remnant is dynamically spherical, although departures from spherical symmetry can occur in the synchrotron emission, through the geometry of the magnetic field and possible dependences of electron acceleration efficiency on the obliquity angle θ_{Bn} between the upstream magnetic field and the shock normal. The SNR dynamics are assumed to be given by the Sedov (1959) self-similar solution for a point blast wave in a uniform medium, although, as will be demonstrated, the appearance of upstream halos is very little

affected by the properties of the downstream fluid. The shock compression ratio is assumed to be 4, its value for a strong shock in a fluid with ratio of specific heats $\Gamma = 5/3$. The magnetic field is assumed to be uniform upstream, oriented at an aspect angle ϕ to the line of sight. Behind the shock, the tangential component of the magnetic field is assumed to be compressed by a factor of 4, so that the magnitude of the magnetic field is enhanced by a factor

$$r_B = \left(\frac{1 + r^2 \tan^2 \theta_{Bn}}{1 + \tan^2 \theta_{Bn}} \right)^{1/2} \tag{1}$$

where r is the shock compression ratio (4 for a strong shock). Thus the postshock synchrotron emissivity takes on an azimuthal dependence which breaks the circular symmetry on the sky. However, the postshock magnetic field (once its total magnitude is calculated from Eq. [1]) is randomized in direction, since SNR radio emission is observed to be polarized at relatively low levels of 10%–15%, indicating that the magnetic field is dominantly disordered behind the shock. In practice this assumption makes almost no difference for the present purposes. I explicitly assume no turbulent amplification of the magnetic field above the maximum factor of 4 for compression where the shock is perpendicular ($\theta_{Bn} = \pi/2$).

Electrons are assumed to be accelerated in the shock wave, attaining a power-law spectrum $N(E) = KE^{-s}$ with $s \sim 2.2$ as observed (see, e.g., Green 1991). Since the process by which electrons are injected into the Fermi mechanism is not understood, no calculations exist for the efficiency of shock acceleration of electrons, or how it might depend on shock velocity or other parameters. Perhaps the simplest assumption, made here, is to take the relativistic-electron energy density to be a specified fraction of the postshock pressure ρv_s^2 with ρ the upstream gas density. I shall assume that fraction is constant except for a possible dependence on shock obliquity. For any one such dependence, the actual value of this efficiency fraction is immaterial since the brightness of the entire image will scale with it. As in FR90, I consider three alternatives for the dependence of the unknown electron-injection process on the obliquity angle θ_{Bn}. They are (1) no dependence ("isotropic" particle acceleration, case I), a preference for quasi-parallel ($\theta_{Bn} \lesssim 45°$) geometries, parameterized by an additional factor $\cos^2 \theta_{Bn}$ (case C), and quasi-perpendicular preference, $\sin^2 \theta_{Bn}$ (case S). (Actually the postshock values of θ_{Bn} are used; a more detailed justification is found in FR90.) In FR90 it was concluded that observations of 10 bright SNRs ruled out case I and favored case S over case C somewhat; however, for breadth of illustration, all three models remain alive here. Behind the shock, electrons are assumed not to diffuse at all; they remain with the fluid element in which they originally appear, and lose energy adiabatically as that element expands. As the shock slows down and the postshock pressure decreases, newly accelerated electrons achieve a lower energy density than was true at earlier times; but earlier accelerated electrons have suffered adiabatic losses, largely compensating, and producing an electron distribution roughly independent of radius. (See Reynolds & Chevalier 1981 for calculated profiles.)

It should be noted that the assumption that the electrons are produced by shock acceleration is not essential. It is merely required that they be suddenly produced at some radius, as the

sharp rims of many SNRs attest. The "isotropic" models should be appropriate to describe the upstream halos expected from any such alternative process, although the sharp rims do provide what seems to me to be strong circumstantial evidence in favor of the shock acceleration process. The only major competitor seriously discussed in the literature is that of second-order Fermi (turbulent or stochastic) acceleration in the remnant interior (e.g., Cowsik & Sarkar 1984), which seems on morphological grounds more appropriate for a remnant like Cas A with a broad, irregular ridge of radio emission in the profile, and no sudden turnon at the edge. The models described here are probably not appropriate for Cas A.

Upstream electron densities are given by one of two analytic prescriptions. In both cases the distribution is continuous at the shock wave. For a simple, discontinuous, plane shock, in which the upstream diffusion coefficient D is constant in space, the particle distribution ahead of the shock will be exponential with an e-folding distance of the diffusion length $r_D \equiv D/v_s$, for particle energies far above thermal (e.g., Blandford & Eichler 1987):

$$N(E, r) = K_0 E^{-s} e^{(r-r_s)/r_D} \tag{2}$$

where r_s is the shock radius. I refer to this as the "exponential" case. If, however, the waves are generated by the particles themselves, as long as the wave amplitudes remain small ($\delta B/B \ll 1$), the distribution falls off much more slowly ahead of the shock. The result is

$$N(E, r) = K_0 E^{-s} \left(1 + \frac{r - r_s}{r_D} \right)^{-1} \tag{3}$$

(Bell 1978). I refer to this case as the "Bell" case. If the wave amplitudes are not small, nonlinear effects become important, and the above quasi-linear result may not be valid. However, it provides a neat parameterization and probably an upper bound to the extent of preshock particle diffusion. I thus expect that the exponential and Bell cases bracket the situation one actually expects in young SNRs. The reader is reminded that both expressions apply to plane shock waves, so are appropriate only relatively close to the shock, $(r - r_s) \ll r_s$.

I shall make the simplest assumption relating the diffusion coefficient D to the MHD (Alfvén) dimensionless wave intensity $\mathscr{I}(k) \equiv (\delta B/B)^2$ in resonant fluctuations, namely, that electrons interact resonantly with waves whose wavelength is of the order of their gyroradius $r_g \equiv \gamma m_e c^2/eB$, and that the (energy-dependent) mean free path $\lambda \cong r_g \mathscr{I}^{-1}$ for diffusion along the magnetic field. Thus the resonant wavevector $k \sim 2\pi/r_g$. I assume no cross-field diffusion at all. (See ABR for similar estimates and notation.) To within factors of order unity, and in the long wavelength limit (wave frequency $\omega \ll$ gyrofrequency Ω_g), we can write

$$D \equiv \frac{\lambda c}{3} = \frac{\lambda_\parallel c}{3} \cos^2 \theta_{Bn} \sim \frac{r_g c}{3} \cos^2 \theta_{Bn} \left(\frac{\delta B}{B} \right)^{-2}, \tag{4}$$

and the diffusion length is given by

$$r_D \equiv \frac{D}{v_s} \sim \frac{r_g c}{3 v_s} \cos^2 \theta_{Bn} \left(\frac{\delta B}{B} \right)^{-2}. \tag{5}$$

Here γ is the Lorentz factor of the electrons; for magnetic fields of order 10^{-4}–10^{-5} G, as expected in SNRs (see, e.g., Reynolds 1988 for a review), centimeter-wave radio emission implies $\gamma \sim 10^3$–10^4. Upstream, where we expect $B \sim 3 \times 10^{-6}$ gauss, electron energies are correspondingly higher, implying upstream gyroradii of order 10^{13} cm. These are the length scales over which we observe the diffusive properties of the preshock medium. Equation (3) is the central relation connecting observations, which constrain D as I show below, with the scattering properties of the upstream medium described by the turbulent wave amplitude δB.

While our attention is mainly directed upstream of the shock, the visibility of the halo may depend on certain downstream details. For SNRs younger than a few thousand years, the reverse shock which moves into the original SN ejecta has not yet reached the center and disappeared. However, the magnetic field in the ejecta is just that of the progenitor star, greatly diluted, barring unexpected turbulent magnetic-field generation in the ejecta themselves. (The shocked ejecta/shocked ISM interface, or contact discontinuity, is another matter.) Thus I show models with a parameter r_{crit} within which the emissivity has been set to zero. This radius is roughly that of the contact discontinuity.

These assumptions fix the emissivity at any volume element ahead of or behind the shock. The plane-shock expressions for the preshock particle densities become increasingly poor approximations at preshock distances comparable to the remnant radius, so that details of the calculated emission at such distances should be regarded with suspicion. However, if emission that far in front is significant, I shall show that the overall morphology is so unusual that it can be ruled out independent of details.

I then integrate along each line of sight the synchrotron emissivity

$$j_\nu = C(s)KB^{(s+1)/2}\nu^{(1-s)/2} \qquad (6)$$

(e.g., Pacholczyk 1970), where $C(s)$ is a constant depending only on the power-law index s, related to the observed synchrotron spectral index α by $s = -2\alpha + 1$, with the observed flux $S_\nu \propto \nu^\alpha$. The frequency provides only an overall scaling factor, but it is assumed to be sufficiently high that internal Faraday rotation in the remnant interior can be neglected. (This assumption affects only the internal polarization, with which we are not concerned, but it speeds up the numerical calculations by a substantial factor.) Profiles along a single radial cut will be shown, as well as full two-dimensional images of predicted synchrotron morphology.

3. RESULTS

3.1. *Profiles*

The full parameter space I have sketched has at least five dimensions: the type of particle acceleration model [three values, isotropic (I), quasi-parallel (C), and quasi-perpendicular (S)]; the type of upstream distribution [two values, exponential (E) or Bell (B)]; the diffusion length $r_D \equiv D/v_s$; the aspect angle ϕ; and the resolution with which the radio image is observed. However, the basic properties of the synchrotron precursor can be illustrated with a few one-dimensional profiles. These describe models with a very thin emission region, suitable for modeling certain thin features in supernova remnants, and which show most clearly the qualitative behavior of the precursor. I have assumed $r_{crit} = 0.95r_s$ to obtain this thin region; in this case, the region is so thin that I have taken the emissivity to be constant. The magnetic field has been assumed to increase by a factor 3 in the shock; this is roughly the average increase over the remnant. In a perfectly ordered situation, the magnetic field would increase by a factor r_B given by equation (1). This expression has been used for the two-dimensional images; see § 3.2 below.

In Figure 1, the magnetic field has been oriented so that $\theta_{Bn} = 0$; there are of course only two points on the face of the
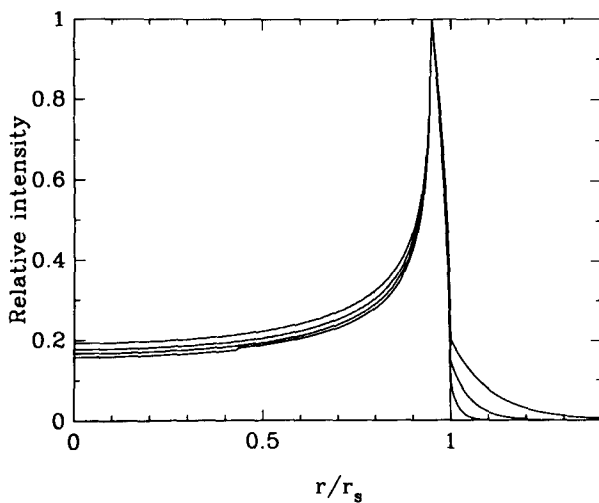
FIG. 1a
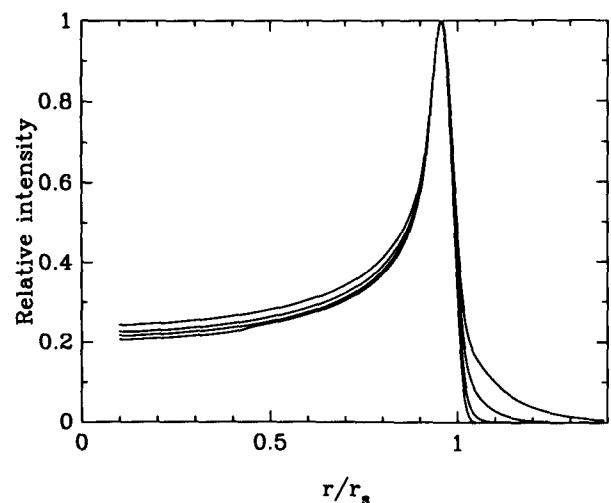
FIG. 1b

FIG. 1.—(a) Exponential profiles, taken along the z-axis (see text). The obliquity angle θ_{Bn} along this direction is zero. The four curves correspond to four values of the relative diffusion length l: *from bottom to top*, 0, 0.02, 0.05, and 0.10. Essentially infinite resolution. (b) As in (a), but convolved to a resolution of 25 beams (FWHM) per shock radius.
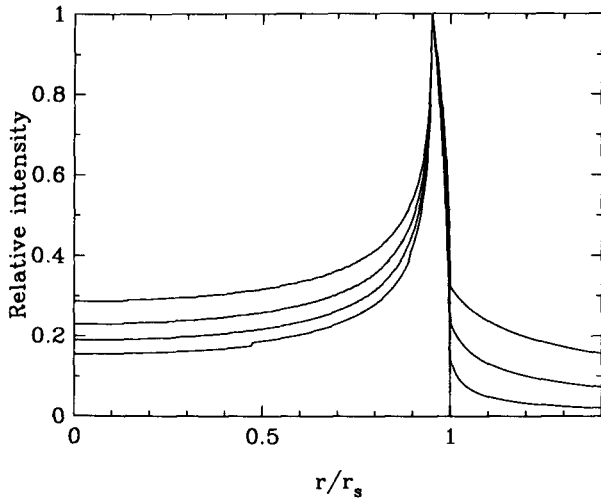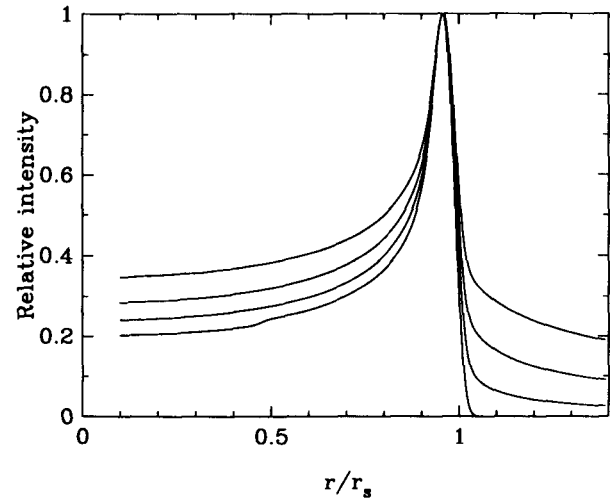
FIG. 2a   FIG. 2b

FIG. 2.—(a) As in Fig. 1a, for Bell profiles. (b) As in Fig. 1b, for Bell profiles.

spherical shock where this is exactly true. However, this figure demonstrates the essential character of the precursor. Figure 1a shows four exponential profiles, for four values of the controlling parameter $l \equiv r_D/r_s$: 0, 0.02, 0.05, and 0.10. Essentially infinite resolution has been assumed, so the profiles contain an unphysical cusp. The no-diffusion profile shows a characteristic of these models: the second derivative of the brightness remains negative as the profile descends all the way to zero at the shock. This will be masked by finite resolution, of course, but it is important because the presence of the precursor for $l > 0$ causes a point of inflection at the shock. Even at finite resolution, as in Figure 1b where the fractional resolution (ratio of beam FWHM to remnant radius) is 0.04, the inflection in the profile is very near the shock radius. This inflection can be taken to locate the shock, then, in observed profiles, as long as
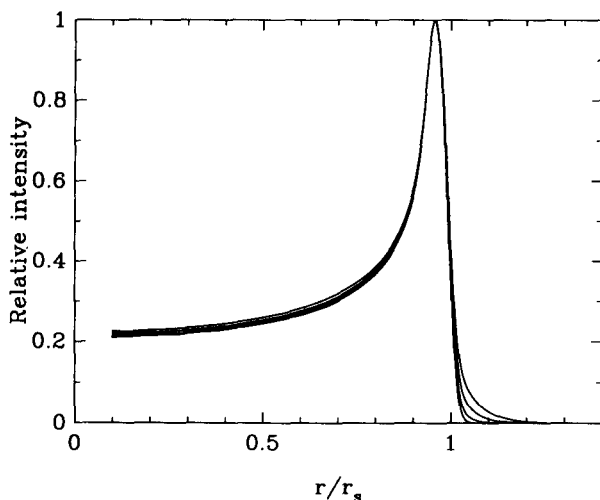
the emissivity appears to rise fairly suddenly, as is the case with several historical shell remnants (Tycho [Dickel, van Breugel, & Strom 1991], Kepler [Dickel et al. 1988], SN 1006 [Reynolds & Gilmore 1986]) as well as other bright remnants (W49 B [Moffett & Reynolds 1994], 3C 397 [Becker, Markert, & Donahue 1985]). Cas A is a notable exception in this regard as in many others.

Figures 2a and 2b show two sets of four profiles each, as in Figure 1 except that here the preshock distribution is that of Bell. The synchrotron precursor is much more obvious, as one would expect, since the relativistic-electron density falls off considerably more slowly with distance ahead of the shock. Again, the inflection point locates the shock quite accurately. The extent of the precursor can be described with a parameter $l_{1/2}$, the distance beyond the inflection over which the profile drops to one-half its value at the inflection point. This quantity was used to compare observed remnants and models in ABR.

If the aspect angle is less than 90°, the relative contribution of the precursor will diminish, both because particles do not scatter as far ahead of the shock at the projected edge of the remnant ($r_D \propto \cos^2 \theta_{Bn}$; eq. [5]) but also because the external emissivity $j_{ext} \propto (B \sin \phi)^{1-\alpha}$ drops directly. Figures 3 and 4 show sets of convolved profiles for cases E and B, respectively, for four values of ϕ: 90°, 60°, 45°, and 30°. High-sensitivity radio interferometric observations, with signal-to-noise ratios of 100 to 1, are not uncommon, and even for small values of ϕ the precursor should be bright enough to be detectable for some remnants, unless r_D is small enough that the precursor is narrower than the angular resolution of the observations.

For comparison purposes, Figure 5 shows two observed profiles of the remnant of SN 1006 AD (Reynolds & Gilmore 1986), made with the Very Large Array of the National Radio Astronomy Observatory[1] at a frequency of 1.37 GHz and 32″ resolution, corresponding to ~30 beams per 15′ radius. The

FIG. 3.—Exponential profiles: $l = 0.05$, for four values of aspect angle ϕ (=90° − θ_{Bn} along the z-axis): from top to bottom, ϕ = 90°, 60°, 45°, and 30°. Convolved to 20 beams per radius.
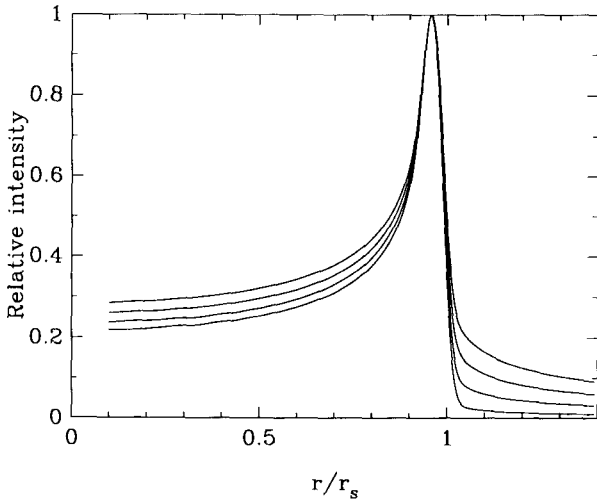
FIG. 4.—As in Fig. 3, for Bell profiles

to understand, as all models (see below) become circularly symmetric as $\phi \rightarrow 0$.

3.2. Model Images

Because the shock obliquity θ_{Bn} varies around the observed periphery of the remnant, profiles such as Figures 1–4 do not give the best idea of the appearance of a SNR radio halo. I have adapted the imaging code described in FR90 and RF90 to include the effects of preshock diffusion, treated as described above. This time the magnetic-field increase at each point on the shock surface has been calculated from equation (1). Particles are assumed to diffuse only radially rather than azimuthally; this approximation becomes poor at about the same distances in front of the shock that the assumption of plane shock geometry breaks down.

Figures 6 and 7 show nine two-dimensional models each; Figure 6 for case E, Figure 7 for case B. All images have been smoothed to an effective resolution of 20 beams per shock radius. In each figure, for each of the three particle-acceleration assumptions I, C, and S, three values of ϕ are shown: 90°, 60°, and 30°. The projection of the magnetic field on the plane of the sky points up (along z) in each figure. The emissivity is assumed zero inside $r_{crit} = 0.8 r_s$. All models have relative diffusion lengths $l \equiv r_D / r_s = 0.05$. The different acceleration models make different predictions about where in azimuth on the sky the shell emission is brightest and where the halo emission is brightest. The latter always occurs along the magnetic field, so at the top and bottom of the shell emission. The brightness and width of the precursor both decrease as ϕ decreases, so that an unobserved halo in a given SNR can always be attributed to the local magnetic field being almost along the line of sight.

profiles are at position angles (measured as usual counterclockwise from vertical) of ~85° and 135°. The very sharp turn-on of radio emission is apparent, as is the sharp (unresolved) rim of emission at the very edge. The detailed shape of the profile at the outer edge is consistent with the beam shape; no halo is observable in either profile. The peak brightnesses in each profile are ~20 mJy beam^{-1} each, while the noise (3 σ, roughly, or ~3 times the dispersion in off-source pixels) is less than 0.5 mJy. While a very small aspect angle ϕ could diminish the observability of a halo, such an aspect angle would make the well-known bilateral symmetry of SN 1006 very hard

FIG. 5a

FIG. 5b

FIG. 5.—Two observed profiles through the radio image of SN 1006 (Reynolds & Gilmore 1986), at position angles 85° (a) and 135° (b). The image, at 1.37 GHz, had an angular resolution of 32″ or ~30 beams per radius. No halo is apparent.
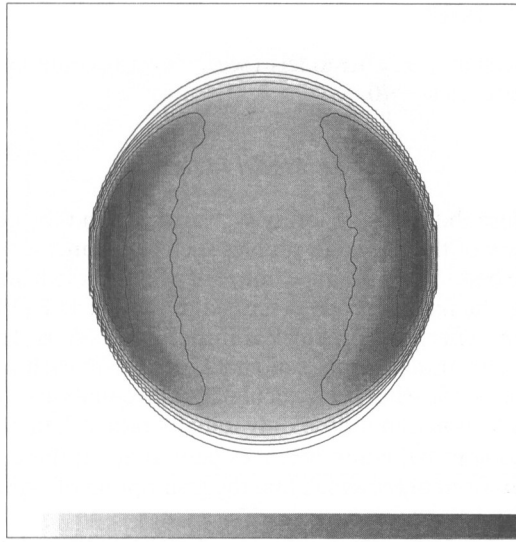
FIG. 6*a*
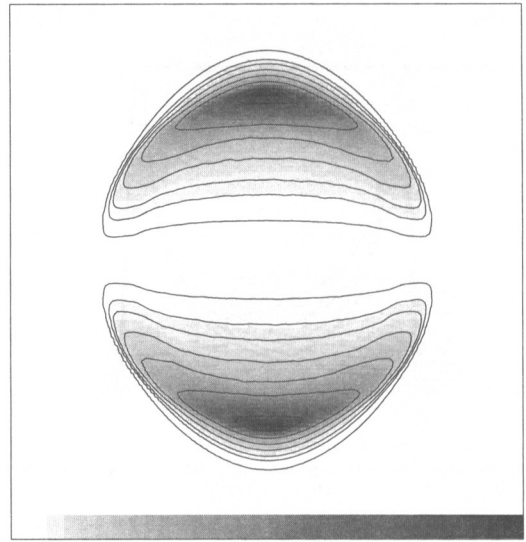
FIG. 6*b*

FIG. 6*c*

FIG. 6*d*
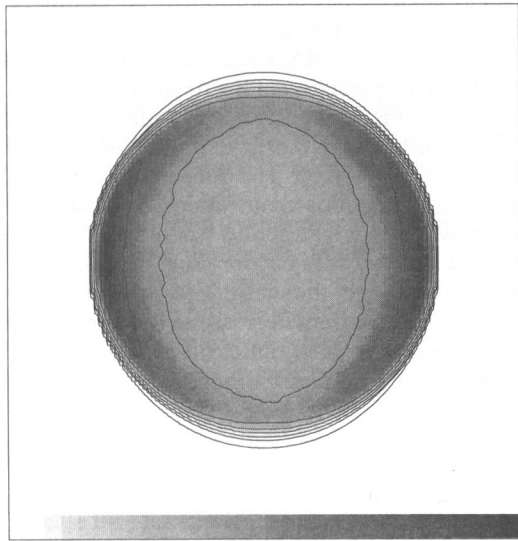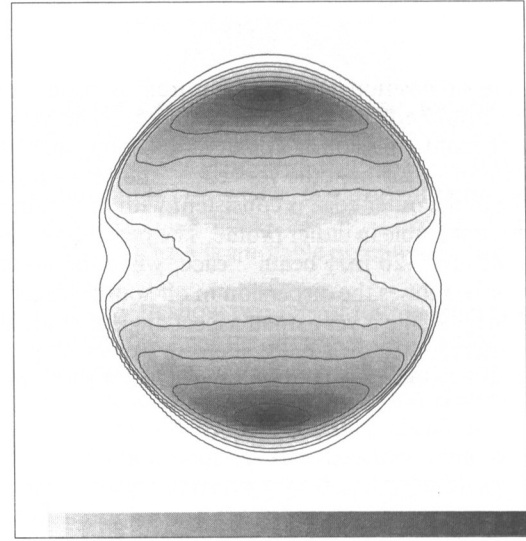
FIG. 6*e*
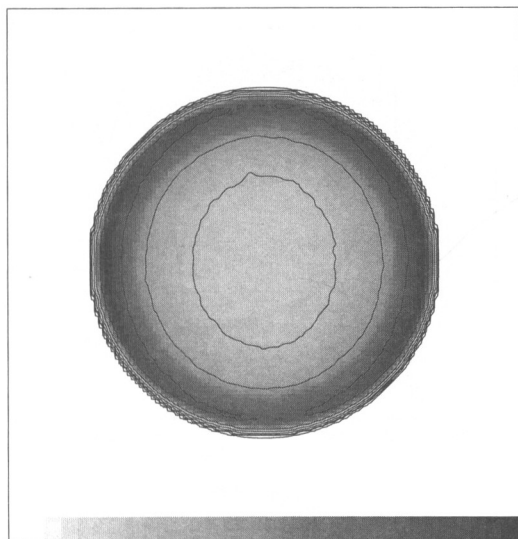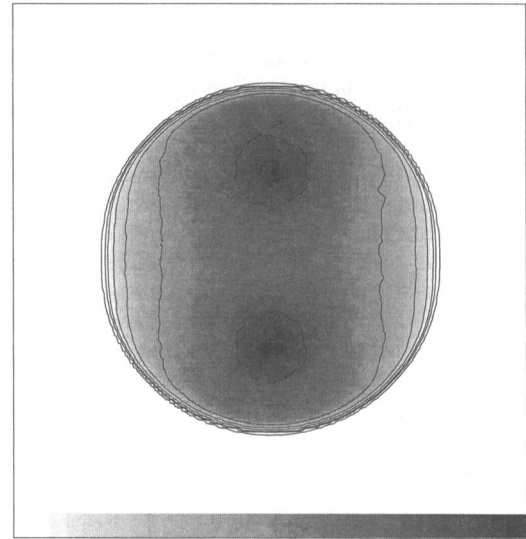
FIG. 6*f*

FIG. 6.—Nine exponential models with $l = 0.05$. (a), case I, $\phi = 90°$; (b), case I, $\phi = 60°$; (c), case I, $\phi = 30°$; (d), case C, $\phi = 90°$; (e), case C, $\phi = 60°$; (f), case C, $\phi = 30°$; (g), case S, $\phi = 90°$; (h), case S, $\phi = 60°$; (i), case S, $\phi = 30°$. Contour levels, in percent of peak, are 1, 3, 5, 10, 20, 40, and 80.
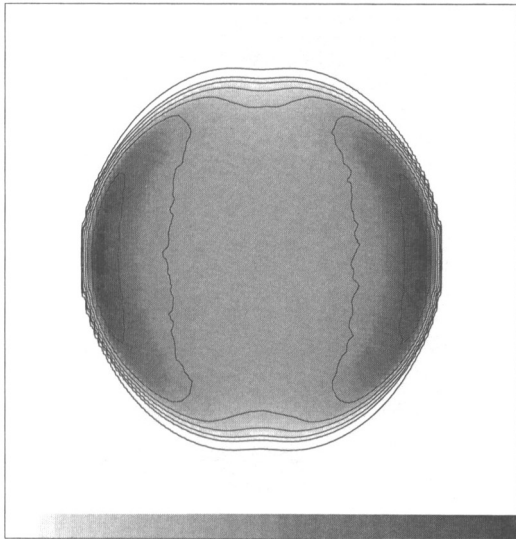
FIG. 6*g*
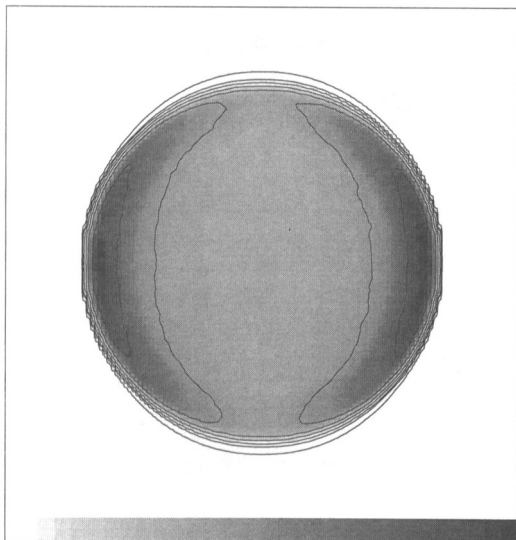
FIG. 6*h*
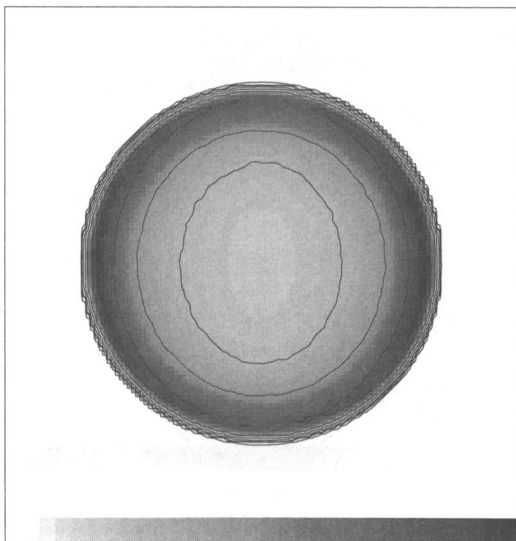
FIG. 6*i*

FIG. 6—*Continued*

At two points on the circumference of each model, no halo at all appears: at these points $\theta_{\mathrm{Bn}} = 0$ and the shock is exactly perpendicular. (Since the sky-plane projection of the magnetic field points up in Figures 6 and 7, those two points are at position angles 90° and 270°.) Thus a single profile showing no halo cannot be taken as evidence against the existence of one. However, a contiguous range of azimuth over which no halo is apparent does constrain the diffusion of electrons. Figure 8 shows four profiles of the model illustrated in Figure 6*h* (exponential, case S, $\phi = 60°$), at position angles 90°, 60°, 30°, and 0°. As the position angle $\rightarrow$ 0, the halo appears clearly, more so since the postshock emission in case *S* is weakest at position angles 0 and 180°.

The value of $l = 0.05$ was chosen because such halos could, in fact, be consistent with radio maps of some young remnants, although in some cases either ϕ must be smaller than 30° or l even less than this. However, the mean free path for 5 GeV cosmic rays in the average interstellar medium is inferred in ABR to be of order 0.1 pc, implying a diffusion length r_D of $c\lambda/3v_s \sim 3$ pc for a shock velocity of 3000 km s^{-1}, probably an upper bound for almost any target SNR. Thus the ISM information implies $l \sim 1$: a diffusion length comparable to the remnant radius (a few parsecs). Figure 9 shows what a SNR would look like for $l = 0.5$, assuming a constant level of turbulence at this ISM value (i.e., an exponential model), for aspect angles $\phi = 90°, 60°$, and 30°. I have taken the isotropic particle-acceleration model, although this doesn't much affect the appearance of the halo. This is the minimal assumption. no excess scattering associated with the shock at all. Figure 9 shows very graphically that this case can be most emphatically ruled out. No SNR in the galaxy resembles any of these images, even those with small values of ϕ.

4. DISCUSSION

We may begin by concluding from Figure 9 that the scattering near SNRs must be considerably enhanced over the mean interstellar value. We dismiss the possibility that for every SNR with well-defined edges, $\phi < 10°$ or so, which is what would be required to cause all synchrotron halos to vanish. [Recall from eq. (5) that the relative diffusion length $l \equiv r_D/r_s \propto 1/(v_s r_s) \propto t^{0.2}$ for Sedov evolution, $r_s \propto t^{0.4}$ and $v_s \propto t^{-0.6}$—so the problem only gets worse with age, albeit slowly.] While details of the assumptions can be contested, the total absence of structures in any way corresponding to the bipolar flares of Figure 9 seems to be conclusive.

The next step, of trying to obtain a measurement or upper limit on l, is more difficult. In most young SNRs, the turn-on of radio emission is essentially unresolved over part of the periphery. These parts could correspond to locations where $\theta_{\mathrm{Bn}} \sim 90°$, where, since we assume the cross-field mean free path is zero, no halo is expected. However, we also note from Figures 6, 7, and 8 that a halo does begin to grow as one moves around the circumference away from those points, so that the angular extent of the region over which a limit can be set may be able to constrain the value of l. See ABR for a fuller discussion of this methodology applied to several young SNRs.

The fact that some of the models of Figures 6 and 7 do not have obviously impossible halos can be used to extract a rough quantitative measure of the increased scattering apparently necessary outside the rims of bright SNRs. Since the diffusion
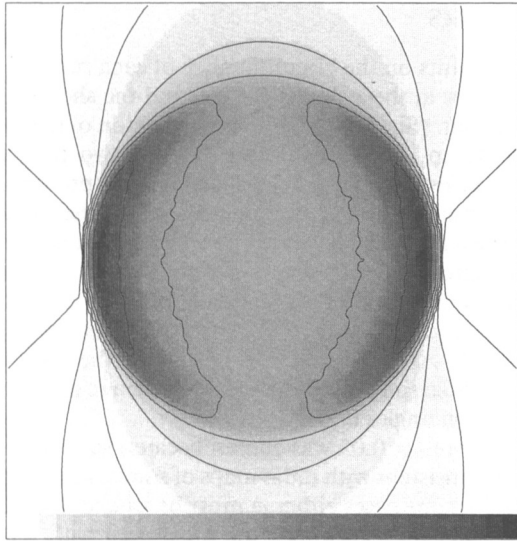
FIG. 7a
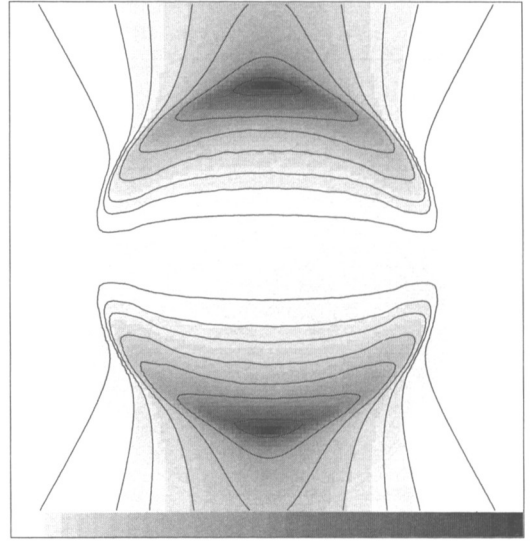
FIG. 7b

FIG. 7c

FIG. 7d
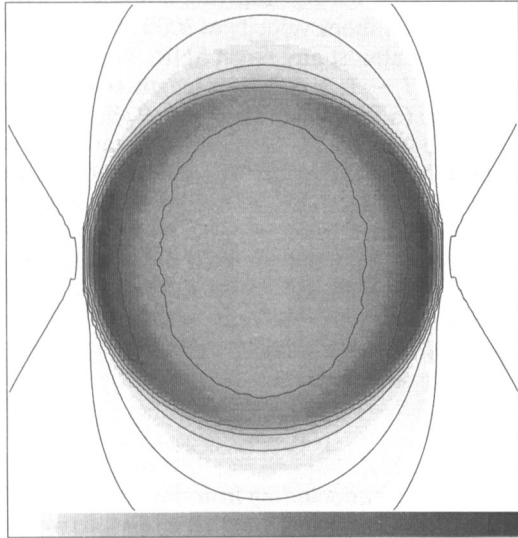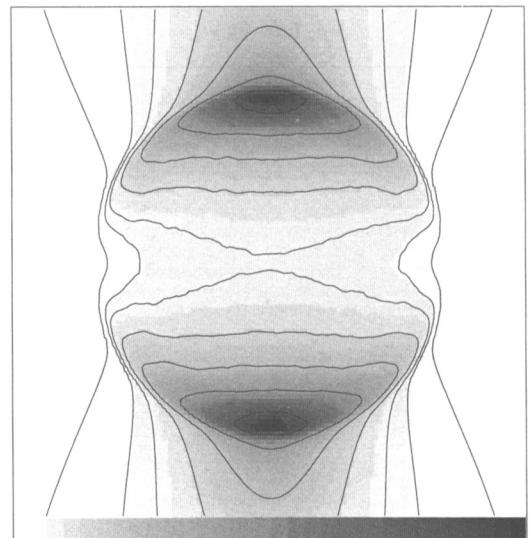
FIG. 7e
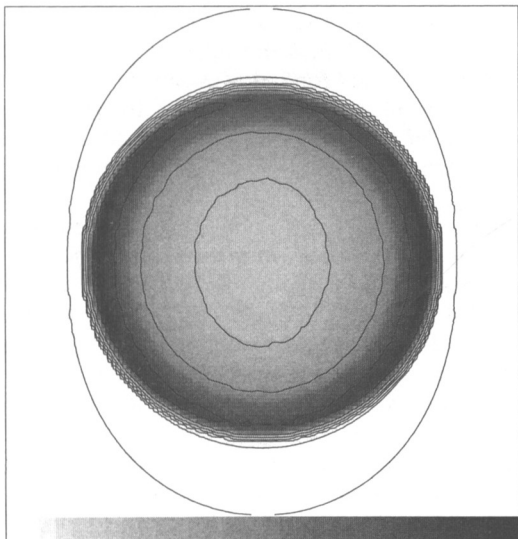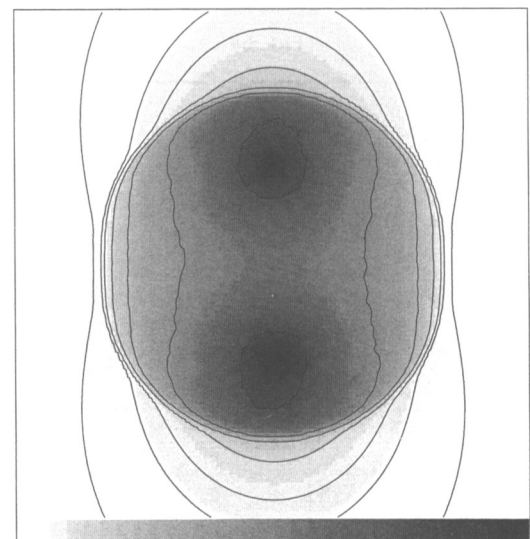
FIG. 7f

FIG. 7.—Nine Bell models, as in Fig. 6. Contour levels as in Fig. 6.
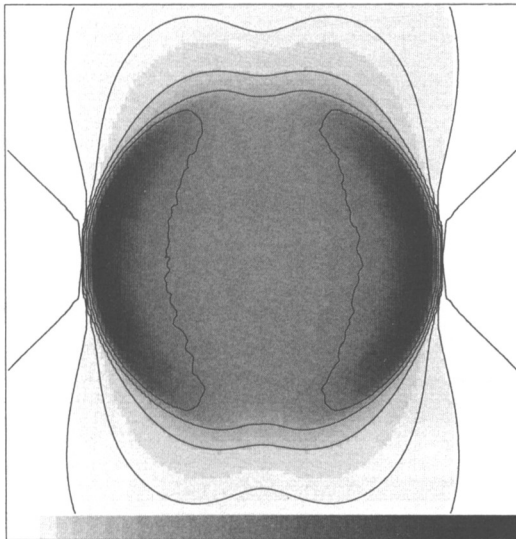
FIG. 7g
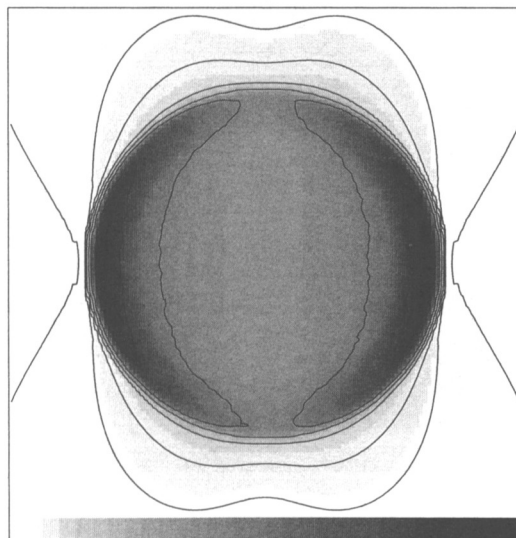
FIG. 7h
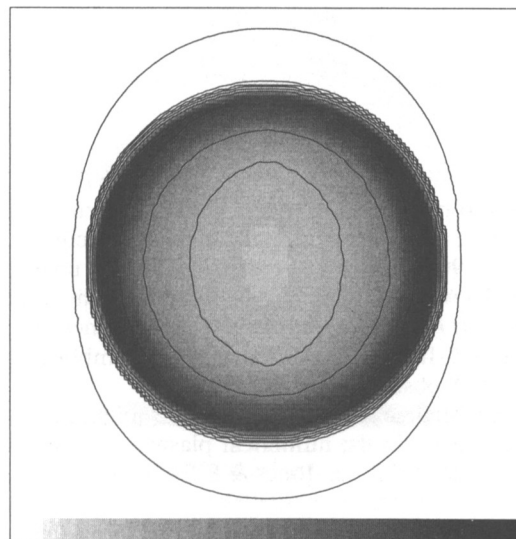
FIG. 7i

FIG. 7—Continued

length in those figures, $0.05r_s$, is 0.1 of that in Figure 9, evidently the scattering mean free path is of order 0.1 times its ISM value or less. The only way to escape this general conclusion is to assert that shock acceleration occurs in virtually no observed SNR, or that for any in which it does, the exterior magnetic field lies quite close to the line of sight. A more rigorous estimate requires a closer look at the form of the profiles exhibited above.

At a particular location on the remnant circumference, the extent of the precursor as shown in the profiles of Figures 1–4 can be quantified. The exponential profiles are quite close to pure one-dimensional exponentials, as one might expect. Define a coordinate system in which x points toward the observer, and y toward the right and z up in the sky plane. The profiles can be considered to be cuts along the z-axis. The major contribution to the emissivity along a single line of sight outside the shock comes where that line of sight passes closest to the remnant (pierces the sky plane; $x \sim 0$). Along that single radius, of course, the particle distribution, and hence the emissivity distribution, is exactly exponential. Thus one can calculate that for this case $l_{1/2} = r_D/\ln 2$.

For the Bell profiles, particle density drops off sufficiently slowly that some account must be taken of the varying path lengths along different lines of sight over which appreciable emissivity is produced. Along each line of sight the emissivity will peak where $x = 0$, and will have a half-width at half-peak $x_{1/2}$ which grows with z. Define $u \equiv z/r_s$, $w \equiv x/r_s$, and (as before) $l \equiv r_D/r_s$. We can then write

$$j_\nu = j_0\left[1 + \frac{(u^2 + w^2)^{1/2} - 1}{l}\right]^{-1} \qquad (7)$$

where $j_0 \equiv j_\nu(r = r_s)$. Now we expect $l \ll 1$, but u and w are both of order unity. From equation (7), for a fixed $u > 1$, j_ν drops to half its $w = 0$ value at

$$w_{1/2} = [(l + 2u - 1)^2 - u^2]^{1/2}, \qquad (8)$$

or, defining $\epsilon \equiv u - 1$,

$$w_{1/2} = (l^2 + 4\epsilon l + 3\epsilon^2 + 2\epsilon + 2l)^{1/2}. \qquad (9)$$

Since we expect both ϵ and l small, as will be shown below, to lowest order

$$w_{1/2} \simeq \sqrt{2}(l + \epsilon)^{1/2}. \qquad (10)$$

We then approximate $I_\nu \simeq j_\nu(2w_{1/2})$ which gives, since $j_\nu = j_0(1 + \epsilon/l)^{-1}$,

$$I_\nu(\epsilon)/I_\nu(\epsilon = 0) = \left(1 + \frac{\epsilon}{l}\right)^{-1/2}. \qquad (11)$$

We readily find, then, that the intensity drops to a fraction f of its value at r_s in a distance

$$\epsilon(f) = l\left(\frac{1}{f^2} - 1\right), \qquad (12)$$

or in particular $\epsilon(1/2) \equiv l_{1/2} = 3l$. This has been tested against
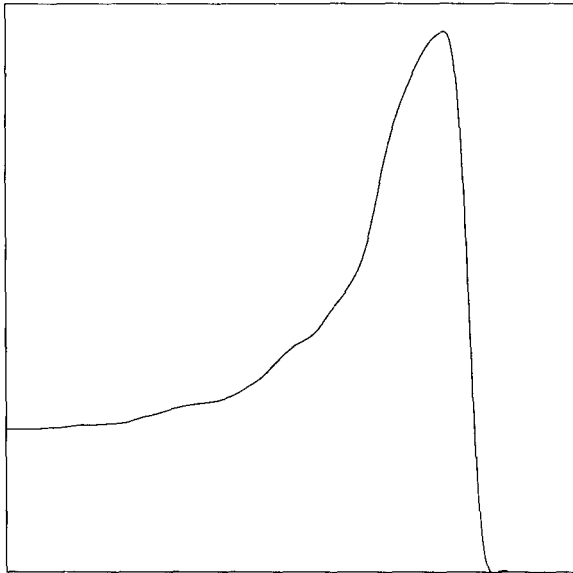
FIG. 8a
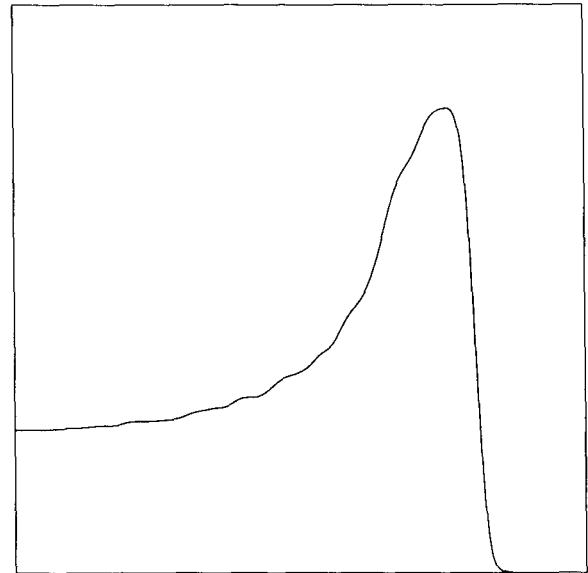
FIG. 8b
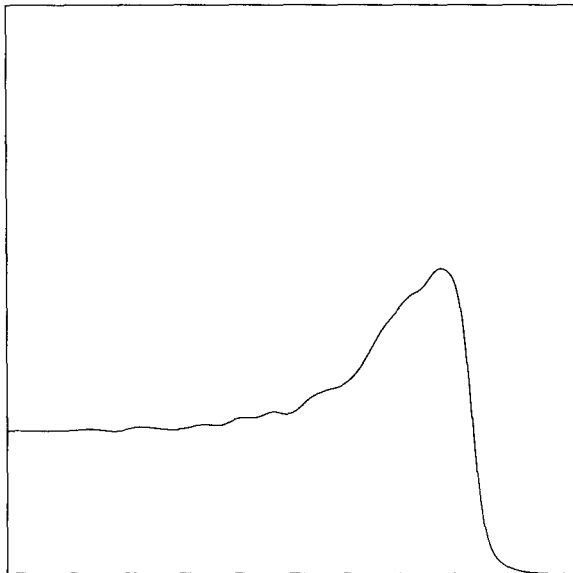
FIG. 8c
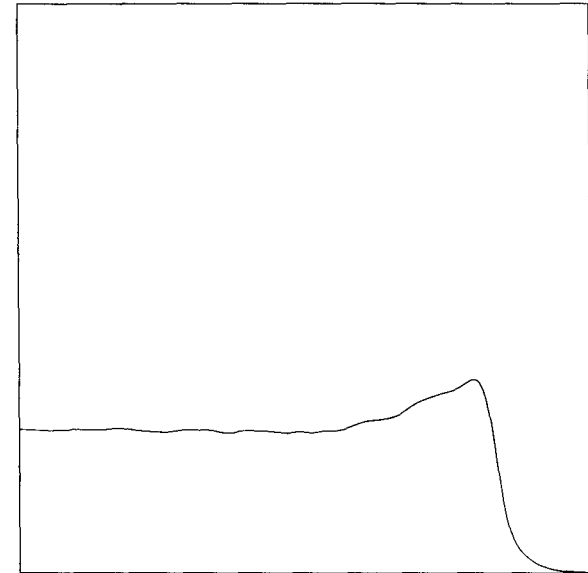
FIG. 8d

FIG. 8.—Four profiles through the model shown in Fig. 6h: exponential, case S, $\phi = 60°$. (a), P.A. 90°; (b), P.A. 60°; (c), P.A. 30°; (d), P.A. 0.

numerically integrated profiles over a range of l from 0.005 to 0.1, and agrees within 70% (30% for $l > 0.02$).

For both cases, then, we can write $l_{1/2} = ar_D$ with a of order unity. Choosing $a = 1$, in fact, is probably a conservative choice, being closer to the exponential than to the Bell values, though, as shown by ABR and above, a constant value of turbulence equal to the mean interstellar value for 5 GeV cosmic rays can be emphatically ruled out, so that in all likelihood the preshock particle distribution, being scattered by self-generated waves, drops off considerably more slowly than exponentially. This result then ties the observed quantity $l_{1/2}$ to the theoretical quantity $r_D \propto (\delta B/B)^{-2}$, enabling the results of ABR, where it was concluded that $\delta B/B \gtrsim (0.03 - 0.2) \times \cos^2 \theta_{Bn}$ for each of four SNRs unless $\phi < 42°$ for all four,

and $\phi < 10°$ for two, based on upper limits to $l_{1/2}$. This limit was found to hold over substantial ranges of azimuthal angle on the sky ψ, not only at individual points where one might have $\theta_{Bn} \sim 90°$, allowing the conclusion that unless all the aspect angles were below the limits mentioned, the wave intensity $\mathcal{I} = (\delta B/B)^2$ is greater than at least 40 times its value in the mean ISM. In no case was a structure resembling the halos of Figures 6–8 observed.

There is of course no reason that $\delta B/B$ might not be much larger than these limits; numerical plasma simulations (e.g., Giacalone et al. 1992; see Jones & Ellison 1991 for a review) show that at least quasi-parallel shocks are accompanied by strong, nonlinear turbulence, $\delta B/B \sim 1$. If this is the case, the quasi-linear results (3), (4), and (5) we have used are of course
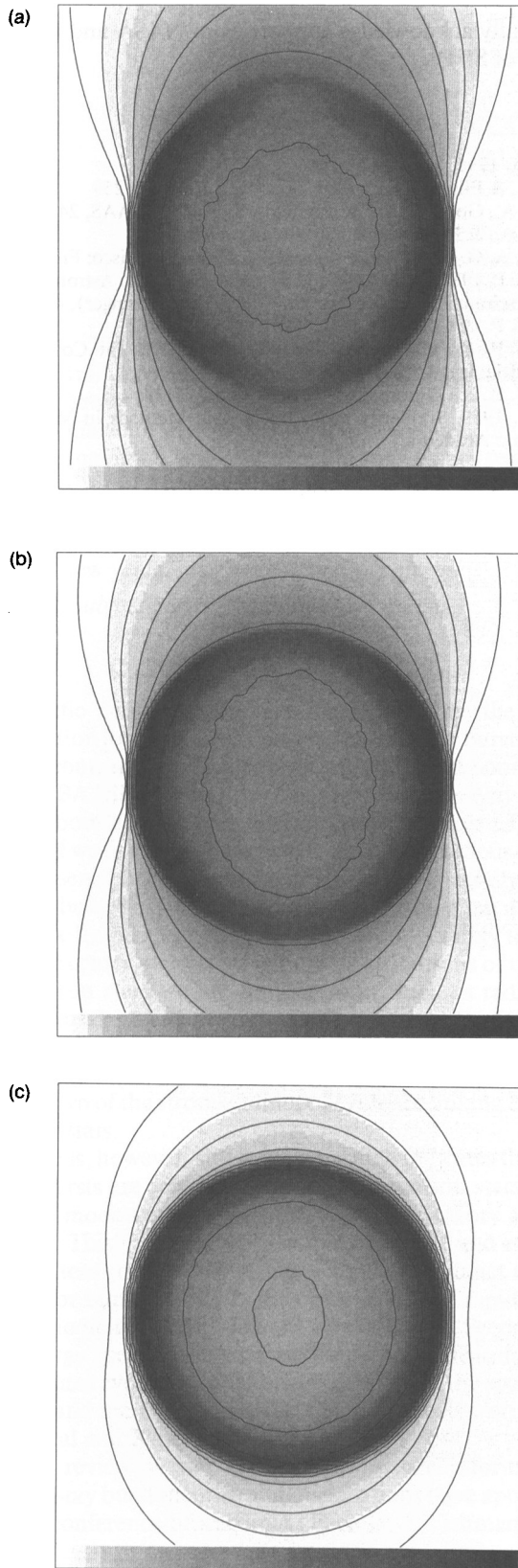
FIG. 9.—Models without local enhancements of MHD turbulence: exponential particle distribution (appropriate for constant level of turbulence), case I, $l = 0.5$, a conservative lower bound to the ISM value. (a) $\phi = 90°$; (b), $\phi = 60°$; (c), $\phi = 30°$. Note the preposterous halos for all three values of aspect angle. Contour levels as in Fig. 6.

invalid, validating the conclusion that young SNRs are surrounded by turbulence, at least for wavelengths of order 10^{13} cm, far stronger than in the average ISM, and presumably associated with the shock as predicted by nonlinear theories of diffusive shock acceleration.

5. CONCLUSIONS

The theory of diffusive shock acceleration unambiguously predicts the existence of synchrotron halos outside the shocks of young SNRs, which might be marked by the sudden appearance of the bulk of the radio emission or by X-ray emission where bulk plasma is apparently heated. I have presented calculated profiles and images of such halos under a range of fairly sensible assumptions about particle acceleration and the properties of the magnetic fields external to the remnant and behind the shock. Several significant conclusions present themselves:

1. The point of inflection of the outer radio profile can provide a good marker for the shock location in any picture in which the synchrotron emissivity arises fairly abruptly at some radius, whether through shock acceleration of electrons or some other process.

2. An observational measure of the extent of the precursor is $l_{1/2}$, the distance in the radial profile beyond the inflection point over which the radio intensity drops by a factor of 2 from its value at the inflection point. This quantity is directly related to $\mathcal{I} = (\delta B/B)^2$, the dimensionless intensity in MHD waves with wavelengths of order the gyroradius of radio-emitting electrons upstream, $\sim 10^{13}$ cm.

3. For many ranges of parameters, the halos predicted do not resemble observed structures commonly found among SNRs. Evidently they are suppressed, either by strong scattering implying high values of $\mathcal{I}$ in the shock vicinity, or because the exterior magnetic field lies nearly along the line of sight. Creative geometries for nonconstant exterior magnetic field may also permit the limits to be avoided.

4. Quantitative lower limits to $\delta B/B$ can be found from observed limits to $l_{1/2}$, which are usually of the order of the angular resolution of the observations.

I hope that these simple simulations of shock precursors spur some observers to try to resolve halos or improve upper limits. If the sharp features often seen near the edges of young SNRs (e.g., SN 1006; Reynolds & Gilmore 1986) are common, their surface brightness may be high enough that they are detectable even with very high angular resolution. The arcs in SN 1006 have been seen at 3 times higher resolution than reported in Reynolds and Gilmore 1986 (Moffett, Goss, & Reynolds 1992), allowing an improvement in the inference of $\delta B/B$ of $3^{1/2}$. If observations can be undertaken at a range of frequencies, limits can be set on magnetic fluctuations over a range of linear scales, although that range unfortunately scales only as the square root of the frequency range.

The model-imaging method of studying the physics of SNRs can be extended to investigate many other issues of importance in particle acceleration and collisionless shock physics. Often fairly robust conclusions can be drawn in spite of the somewhat irregular morphology of the typical SNR at radio wavelengths. These calculations can best be employed in interaction with high-resolution, high-intensity radio observations.

More of these are necessary and should pay substantial scientific dividends.

REFERENCES

Achterberg, A., Blandford, R. D., & Reynolds, S. P. 1993, A&A, in press (ABR)

Becker, R. H., Markert, T., & Donahue, M. 1985, ApJ, 296, 461

Bell, A. R. 1978, MNRAS, 182, 147

Blandford, R. D., & Eichler, D. 1987, Physics Repts. 154, 1

Blandford, R. D., & Ostriker, J. P. 1978, ApJ, 221, L29

Cowsik, R., & Sarkar, S. 1984, MNRAS, 207, 745

Dickel, J. R., Sault, R., Arendt, R. G., Matsui, Y., & Korista, K. T. 1988, ApJ, 330, 254

Dickel, J. R., van Breugel, W. J. M., & Strom, R. G. 1991, AJ, 101, 2151

Fulbright, M. S., & Reynolds, S. P. 1990, ApJ, 357, 591 (FR90)

Giacalone, J., Burgess, D., Schwartz, S., & Ellison, D. C. 1992, Geophys. Res. Lett., 19, 433

Green, D. A. 1991, PASP, 103, 209

Jones, F. C., & Ellison, D. C. 1991, Space Sci. Rev., 58, 259

Moffett, D. A., Goss, W. M., & Reynolds, S. P. 1992, BAAS, 24, 1232

Moffett, D. A., & Reynolds, S. P. 1994, in preparation

Pacholczyk, A. G. 1970, Radio Astrophysics (San Francisco: Freeman)

Reynolds, S. P. 1988, in Galactic and Extragalactic Radio Astronomy, ed. G. L. Verschuur & K. I. Kellermann (New York: Springer), 439

Reynolds, S. P., & Chevalier, R. A. 1981, ApJ, 245, 912

Reynolds, S. P., & Fulbright, M. S. 1990, in Proc. 21st. Int. Cosmic Ray Conf. (Adelaide), 4, 72 (RF90)

Reynolds, S. P., & Gilmore, D. M. 1986, AJ, 92, 1138

Sedov, L. I. 1959, Similarity and Dimensional Methods in Mechanics (New York: Academic)